Low- and High-Density Unknown Waters at Ice–Water Interfaces

AUTHOR NAMES.
Hiromasa Niinomi[*†,‡], *Akira Kouch*[†], *Tetsuya Hama*[§], *Hiroki Nada*[¶], *Tomoya Yamazaki*[†] *and Yuki Kimura*[*†]

AUTHOR ADDRESSES
[†] Institute of Low Temperature Science, Hokkaido University, Kita-19, Nishi-8, Kita-ku, Sapporo, 060-0819, Japan
[‡] Institute of Multidisciplinary Research for Advanced Materials, Tohoku University, 2-1-1 Katahira, Aoba-ku, Sendai, 980-8577, Japan
[§] Komaba Institute for Science, the University of Tokyo, 3-8-1 Komaba, Meguro, Tokyo 153-8902, Japan
[¶]National Institute of Advanced Industrial Science and Technology (AIST), 16-1 Onogawa, Tsukuba 305-8569, Japan

* Corresponding Authors: Hiromasa Niinomi (HN) and Yuki Kimura (YK)
Email: hiromasa.niinomi.b2@tohoku.ac.jp (HN), ykimura@lowtem.hokudai.ac.jp (YK)

ABSTRACT

Experimental confirmation of liquid polymorphs of water, high-density liquid (HDL) and low-density liquid (LDL), is desired not only for understanding the liquid state of matters but also for the origin of the mysterious properties of water. However, this remains challenging because the liquid-liquid critical point of water lies in experimentally inaccessible supercooling conditions known as 'no-man's land'. Here, we show by *in situ* optical microscopy that droplets and layers of a low- and high-density unknown waters (LDUW and HDUW) appear macroscopically depending on ice polymorphs at non-equilibrium interfaces between water and ices under experimentally accessible (de)pressurization conditions. These unknown waters were found to have characteristic velocities (about 20 m/s and 100 m/s for LDUW and HDUW, respectively) different from water (about 40 m/s) and quasi-liquid layers (QLLs) (about 2 m/s and 0.2 m/s for droplet and layer forms of QLL, respectively.). Our discoveries provide insight on liquid polymorphism of water.

39 **TOC Graphic**

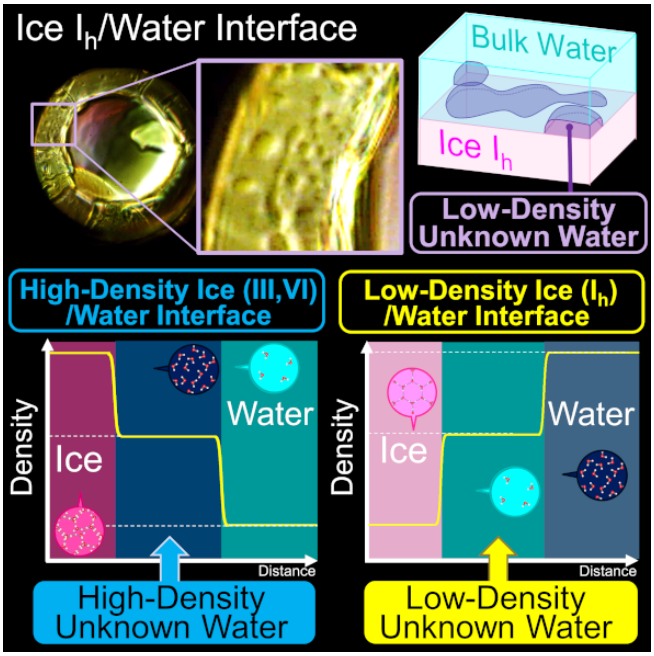

40

Experimental confirmation of polymorphism in single-component liquids is a key to understanding the liquid state of matter[1-3]. Unlike crystalline-state polymorphs, whose which can be well characterized by reciprocal-space analysis because of their long-range ordering, the variety of disordered liquid states is obscured by the lack of clear expressions to characterize their structural signatures. Recent studies have suggested that single-component substances can exist in two or more liquid phases characterized by differences in their density and local ordering; this phenomenon is referred to as liquid polymorphism[3,4]. Phase transformation between liquid polymorphs, i.e. liquid-liquid phase separation (LLPS) or liquid-liquid phase transition (LLPT), has been theoretically predicted in various pure substances including silicon[5], carbon[6], hydrogen[7], and nitrogen[8]. However, experimental confirmation of the phenomenon is exceedingly rare, and a liquid–liquid critical point at which LLPS takes place has not been experimentally confirmed, except in the case of sulphur[1]. This situation is mainly because such LLPTs occur under experimentally difficult conditions involving high temperatures and pressures, or they occur in supercooled regions with inevitable contamination by crystal formation[9]. Such experimental constraints have seriously hindered the progress of research into liquid polymorphism.

Water, which is such an abundant material on the Earth that its phase transitions governs various natural and biological phenomena, is also considered to be a candidate for showing liquid polymorphism as a consequence of the second-critical-point hypothesis[10], which attempts to explain the origins of the various unique properties of water[11], such as its maximum density at 4 °C. In this hypothesis, water is considered to exist as a supercritical state formed from two types of liquid with different densities and local structures: a low-density liquid (LDL) and a high-density liquid (HDL). LLPS of water into LDL and HDL is considered to arise at a liquid–liquid critical point that occurs at a low temperature and a high pressure (Figure 1)[12]. This is because the

64 unique properties of water can be elegantly explained by hypothesizing the existence of this liquid–
65 liquid critical point: the second-critical-point hypothesis[10,13]. This hypothesis has motivated
66 numerous studies on local structure of water at a molecular scale by spectroscopic[14,15], X-ray[16,17],
67 and neutron-scattering experiments[18,19] in the supercritical regime. These studies have supported
68 the hypothesis by suggesting that two structural classes of water fluctuate and change their
69 correlation lengths in supercooled water depending on the conditions near the liquid–liquid critical
70 point[20]. However, no experimental confirmation of a macroscopic LLPS or a LLPT of water has
71 been found. This is because the liquid–liquid critical point of water lies in experimentally
72 inaccessible conditions known as 'no-man's land', where supercooling of liquid is obstructed by
73 rapid crystallization beyond the experimentally accessible time scale[16,17]. Studies on liquid
74 polymorphism in water have been seriously hampered by the constraint imposed by this
75 supercooling limit.

76 We have previously discovered by *in situ* optical microscopy that macroscopic droplets and
77 layers of high-density unknown water (HDUW) separated from bulk water by a clear interface
78 appear at the interface between water and high-density ices (ices III and VI) grown or melted by
79 depressurization or pressurization in a sapphire anvil cell[21]. In the present work, we found that
80 macroscopic droplets and layers of low-density unknown water (LDUW) separated from bulk
81 appear at the interface between water and low-density ice (ice I_h) grown or melted by
82 depressurization or pressurization in an electrically-regulated sapphire anvil cell (see Experimental
83 Methods and Supporting Information (SI) Text S1)[22]. In addition, we determined the ratio between
84 the interfacial tension and the viscosity‑the so-called characteristic velocity. The results confirmed

that LDUW and HDUW differ from previously observed waters, including the quasi-liquid layer observed at air–ice interfaces[23,24].

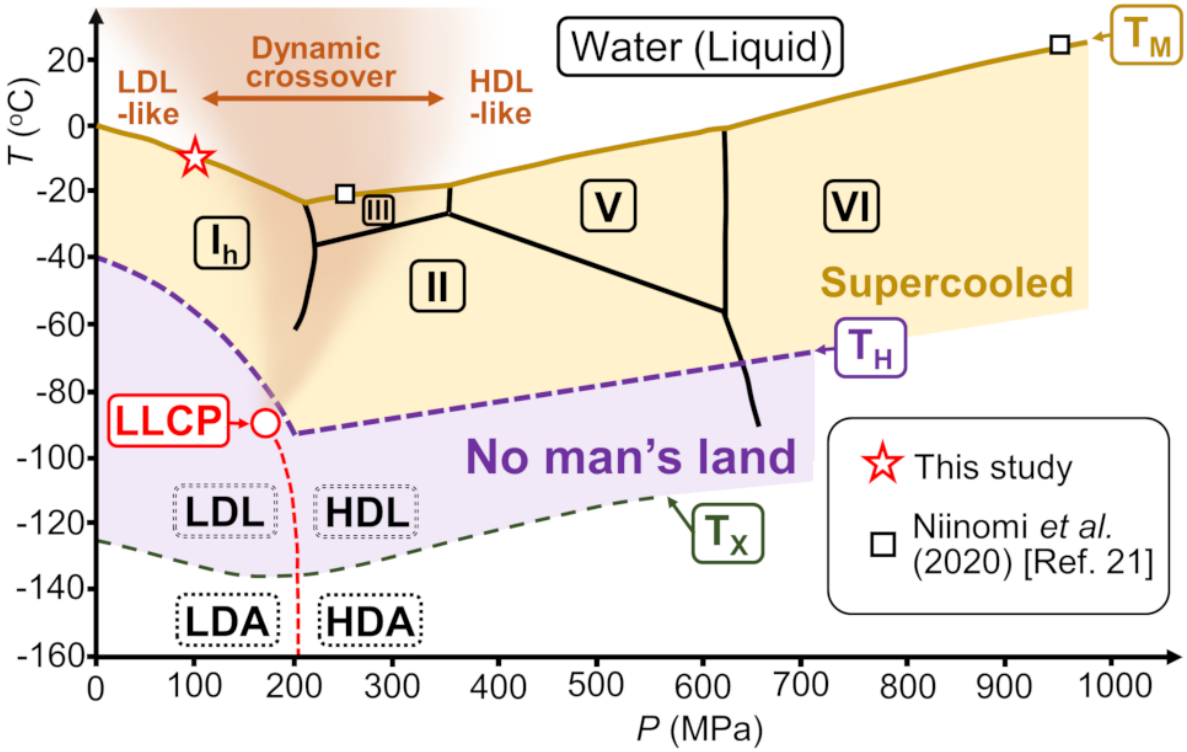

Figure 1. Phase relations of water, and the experimental conditions for the in situ observations of the water–ice interfaces. Phase relations of water and our observation conditions. The red star indicates the conditions for the observations of the water–ice I_h interface in this study. The black squares indicate the conditions for observations of water–high-pressure ice III or ice VI interfaces in a previous study[21]. The solid brown line indicated by T_M shows the melting temperatures of the ices. The liquid water below T_M is metastable supercooled water. The region where supercooled water can exist is highlighted in yellow. The purple dashed line indicated by T_H is the temperature at which homogeneous nucleation inevitably occurs and supercooled water cannot exist because of the supercooling limit; the temperature region below T_H is therefore the so-called 'no-man's land', highlighted in purple. The dashed green line indicated by T_X is the amorphous ice crystallization line. The red circle indicates the liquid–liquid critical point (LLCP). The red dashed line emanating from the liquid–liquid critical point is the expected first-order transition line between LDL (low-density amorphous ice, LDA) and HDL (high-density amorphous ice, HDA) above (below) T_x. The region highlighted in the brownish colour emanating from the liquid–liquid critical point is the region that contains the dynamic crossover lines between LDL-like and HDL-like water, as suggested by previous studies and summarized by Taschin *et al.* [12] The range of this region was depicted by reference to Ref. 12. Stable, metastable, and predicted metastable phases are indicated by the rectangles surrounded black solid, dotted, and dotted double lines, respectively.

Figure 2 shows *in situ* bright-field optical micrographs of the interface between bulk water and ice grown in water by depressurization (see also SI Movie S1). Liquid droplets separated from the bulk water with a clear interface between the water and the growing ice I_h when effective overdepressure of about 2.3 GPa to drive crystal growth was applied at the interface[25] in the electrically-regulated anvil cell (Figure 2, SI Text S2). This overdepressure corresponds to a thermodynamic driving force for crystallization of about 8.6×10^{-21} J. The water–ice interface exhibited a macroscopically smooth morphology before depressurization (Figures 2 **A** 0 s and **B** 0 s) but upon depressurization, it exhibited wavelike pattern (Figures 2 **A** 0.16 s and **B** 0.16 s), resulting in the formation of droplets through breakaway of the tips of the waves (Figures 2 **A** 0.53 s and **B** 0.53 s). This indicated that the substance that exhibited the wavelike pattern was also liquid. The resulting liquid coalesced when a droplet reached a step-like contrast, indicating that this step-like contrast arose from the existence of a thin layer of liquid (Figures 2 **A** 0.73 s and **B** 0.73 s). We confirmed the existence of the thin layer of liquid by *in situ* observation with an optical

microscope equipped with a Fizeau-type laser interferometer (See Materials and Methods and SI Movie S2).

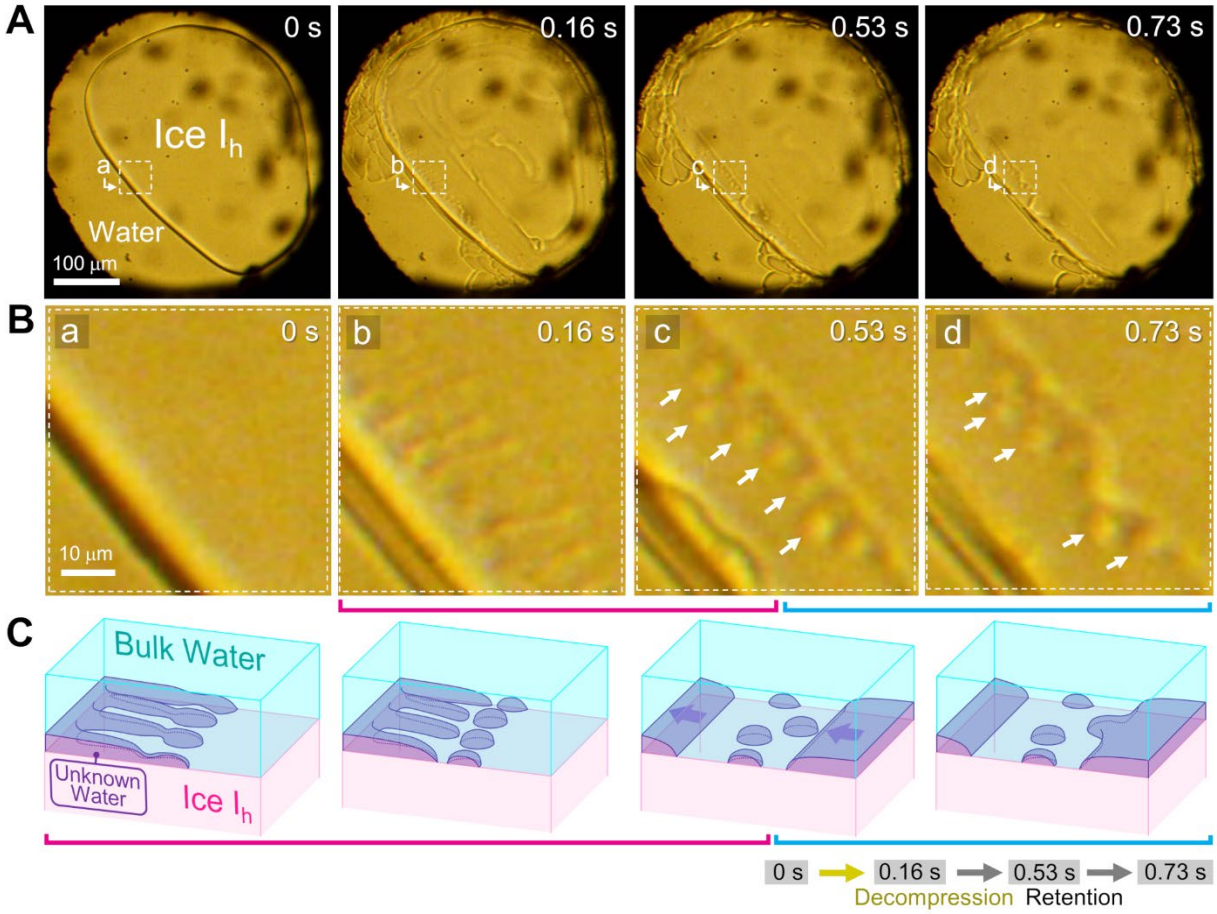

Figure 2. Time-lapse micrographs showing the appearance of LDUW at the interface between water and ice grown by decompression. (**A**) Time-lapse micrographs captured by the *in situ* observations. (**B**) Magnified images of the regions indicated by the white dashed squares denoted by a–d. The white arrows indicate droplets of LDUW. **A** 0 s shows the initial state before decompression. **A** 0.16 s–0.73 s show time-lapse micrographs after decompression. The pressure was maintained in **A** 0.16 s–0.73 s**.** (**C**) Schematics showing the temporal evolution of the morphology of LDUW. The magenta and cyan solid lines indicate the corresponding schematic for the temporal evolution of the morphology shown in micrographs **B** 0.16 s–0.73 s underlined with magenta and cyan solid lines. The yellow and grey arrows in the right-hand bottom corner show the operations of decompression and retention, respectively. See also SI Movie S1.

Observations by interferometric microscopy showed that the wetting liquid layer spread over a wide area of the ice surface, suggesting that its wetting angle was less than 90°. If the wetting angle θ was in the range 90–180° the thickness of the liquid layer (h) would have been unrealistically large on the basis of the following equation for wetting of a substrate by a spherical droplet of radius r:

$$h = r(1 - cos\theta) \qquad (1)$$

Equation (1) suggests that the thickness t is in the range $r < t < 2r$ for $90° < \theta < 180°$. Because $2r$ corresponds to the in-plane size of the liquid layer and this size was 100–200 μm (SI Movie S2), the thickness must have been at least 150–100 μm if the wetting angle is assumed to be more than 90°. This thickness is comparable with the thickness of the sample chamber determined from the thickness of a hole in the gasket after the experiment. However, the observations clearly showed that the thickness of the thin layer was markedly smaller than that of the sample chamber. Therefore, the wetting angle must have been less than 90°. This allowed us to estimate whether the density of the liquid comprising the thin layer was lower than that of bulk water by using Young's equation[26]:

$$\gamma_{IW} = \gamma_{IL} + \gamma_{LW} cos\theta \qquad (2)$$

where γ_{IW}, γ_{IL}, and γ_{LW} are the ice–bulk water, ice–newly discovered liquid, and newly discovered liquid–bulk water interfacial free energies, respectively. From this equation, the constraint $\theta < 90°$ leads to $\gamma_{IW} > \gamma_{IL}$, implying that the structure of the liquid thin layer is more similar to that of ice I_h, (with a lower density than that of bulk water) compared with that of bulk

water. Therefore, the density of the thin layer is probably lower than that of bulk water. Hereinafter, we refer to this unknown liquid at the water–ice I_h interface as 'LDUW'.

Droplets of LDUW were also observed on melting ice I_h (Figures 3 and SI Movie S3). Upon pressurization corresponding to 8.6×10^{-21} J of thermodynamic driving force for melting, droplets separated from the bulk water and a clear interface appeared (Figures 3 **A** 0.10 s and **B** 0.10 s). Initially, some of these droplets had a non-hemispherical elongated shape that changed into a hemispherical shape through splitting into smaller droplets within one second (Figures 3 **A** 0.30 s and **B** 0.30 s). We also observed that moving droplets coalesced within one second, clearly demonstrating their fluid nature. Observations by interferometric microscopy confirmed the existence of a thin layer of liquid when the ice was melted by pressurization (SI Movie S2).

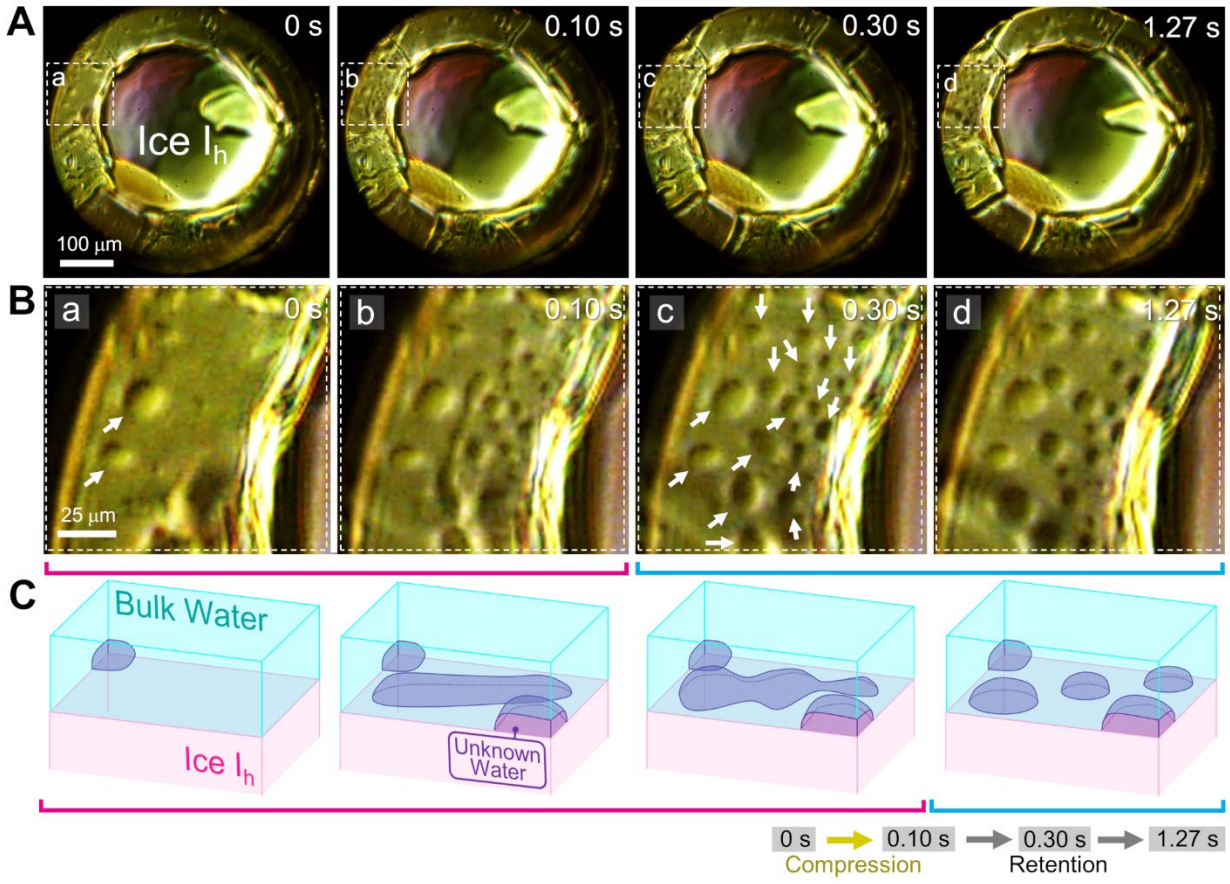

Figure 3. Time-lapse micrographs showing the appearance of LDUW at the interface between water and ice melted by compression. (**A**) Time-lapse micrographs captured by the *in situ* observations. The ice crystal had a ring-like shape because the edge of the disk-like single crystal in contact with the thermally conducting copper gasket tended to grow faster than the central region distant from the gasket. (**B**) Magnified images of the regions indicated by the white dashed squares denoted by a–d. The white arrows indicate droplets of LDUW. **A** 0 s shows the initial state before compression. **A** 0.10 s–1.27 s show time-lapse micrographs after compression. The pressure was maintained in **A** 0.10 s–1.27 s. (**C**) Schematic showing the temporal evolution of the morphology of LDUW. The magenta and cyan solid lines indicate the corresponding schematic of the temporal evolution of the morphology shown in micrographs **B** underlined by magenta and cyan solid lines. The yellow and grey arrows in the right-hand bottom corner indicate the operations of compression and retention, respectively. See also SI Movie S3.

We also succeeded in determining the characteristic velocity of LDUW by analysing the dynamics of coalescence of a small liquid droplet with a liquid thin layer (Figures 4 **A** and SI Movie S4). It is known that the process of coalescence of a small droplet with a large one can be regarded as a weak perturbation of the contact line for the larger droplet. When the contact angle of the droplet is small enough to validate the lubrication approximation ($\theta << 1$ rad)[27], the temporal evolution of the relaxation of the amplitude of the contact lines perturbed by a mode with wave vector q is described by the following equation[28,29]:

$$u_q = u_q(0) exp\left(-\frac{V^*\theta^3 q}{3l}t\right) \qquad (3)$$

where $V^* = \gamma/\eta$ is the characteristic velocity (where γ and η are the interfacial tension and shear viscosity of LDUW, respectively), and $u_q(0)$ is the initial value of the amplitude. The logarithmic factor $l = \ln(L/a)$ is a cutoff parameter to eliminate a singularity at the contact line and at infinite distance; here, a is the molecular size (3.7 Å for water) and L is the approximate size of the larger liquid droplet. From Eq. (3), the relaxation time is given by $\tau_q = 3l/(V^*\theta^3 q)$.

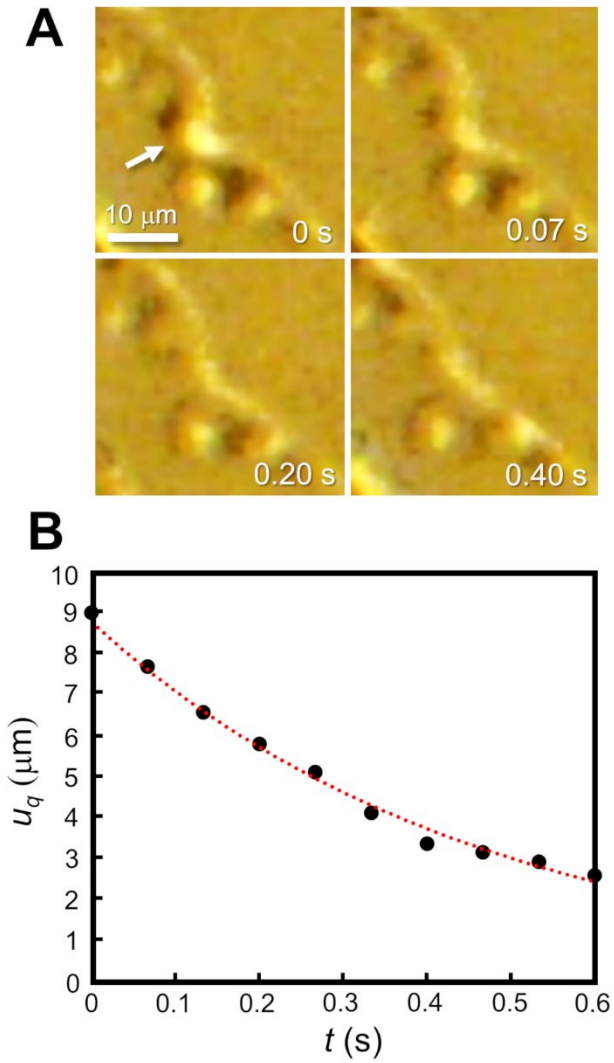

Figure 4. Temporal evolution of the pattern of the contact line during the coalescence of a droplet and a thin layer of LDUW. (**A**) Time-lapse micrographs showing the temporal change in the pattern of the contact line during the coalescence of the droplet and the thin layer of LDUW. The white arrow indicates the droplet coalescing with the thin layer. (**B**) Temporal evolution of the amplitude u_q. The black dots are measured data. The data are fitted well by Eq. (3) (the red dotted line). See also SI Movie S4.

We can regard the thin layer as a large droplet that absorbs the small droplet in the relaxation process. An analysis of the *in situ* microinterferogram showed that the wetting angle was in the range 1.76–1.82° (~0.03 rad), ensuring that the lubrication approximation is valid (See SI Text S3). Figures 4 **B** shows the measured temporal evolution of the amplitude of the contact line in the observation shown in Figures 4 **A**. The measured value was well fitted by Eq. (3), allowing us to calculate the relaxation time to be 0.467 s and $q^{-1} \sim u_q(0)$ to be 8.78 μm. Therefore, V^* is estimated to be in the range 19.3 to 21.2 m/s. This value is one order of magnitude larger than that of a quasi-liquid droplet (~2 m/s) and two orders of magnitude larger than that of a layer on the air–ice interface (~0.2 m/s)[28]. Note that the values for the quasi-liquid layer are based on the interfacial tension for air, whereas that of LDUW is based on that for water. The interfacial tension between liquids with the same composition should generally be smaller than that for air. This leads to the estimation that the characteristic velocity of LDUW should be much smaller than that of the quasi-liquid layer if their viscosities are similar. Nevertheless, the characteristic velocity of LDUW is much larger than that of the quasi-liquid layer, meaning that the viscosity of LDUW must be less than that of the quasi-liquid layer. Therefore, LDUW is distinguishable from the quasi-liquid layer. In addition, the maximum value of the viscosity of LDUW can be estimated to be about 1.6×10^{-3} Pa·s (See SI Text S4), which confirms that LDUW is liquid, because the value is much smaller than that at the glass-transition temperature (10^{12} Pa·s)[30]. This estimated value is also smaller than that of bulk water (~2.3×10^{-3} Pa·s)[31,32] under the conditions of our observations (−10 °C and 107 MPa), (See SI Text S5). These c omparisons confirmed that LDUW is distinguishable from previously observed forms of water.

In situ optical microscopy has previously shown that macroscopic droplets and layers of HDUW appear at the interface between water and high-pressure ices III and VI grown or melted

in bulk water[21]. Thus, the observations in this study showed that both low- and high-density unknown waters can be observed macroscopically at interfaces of water with various ice polymorphs in analogy with the LDL–HDL pair even under conditions far from those of the so-called 'no-man's land' (Figure 1). Although the observation of the low- and high-density unknown waters does not directly show the existence of LDL, HDL and their critical point, signs of transitions between an LDL and HDL have been suggested not only for supercooled water but also for water at temperature above the melting temperature as a dynamic crossover between LDL-like and HDL-like water[13]. Although a dynamic crossover is not a first-order transition, its line is characterized by a change in the slope of the dependency of the physical and structural properties of water, such as its viscosity, spectroscopic stretching band, or rotational correlation time, with pressure or temperature. The pressure region where the dynamic crossover has been suggested to occur ranges from about 150 to 300 MPa[13], where high-pressure ice III is stable if the temperature is below the melting temperature (Figure 1). The structures of ice I_h and ice VI are similar to the local structures of LDL and HDL, respectively, whereas ice III has an intermediate structure[20,33-36] (Figure S7). These relationships imply a relationship between the region of dynamic crossover and the stable regions of ices, leading to a relationship between the pair of LDL-like and HDL-like waters above the melting temperature and the LDUW–HDUW pair. This relationship can be inferred not only from the local structure, but also from the physical properties. Our analysis of the dewetting dynamics of HDUW at the water–ice III interface showed that its characteristic velocity is about 100 m/s (See SI Text S6 and SI Movie S5). This value is roughly an order of magnitude larger than that for LDUW, suggesting that LDUW is much more viscous than HDUW. This is consistent with the relationship between the LDL and HDL forms predicted by a molecular-dynamics simulation, which suggested that the viscosity of LDL is an order of magnitude larger

than that of HDL near the estimated conditions for the LDL–HDL first-order transition (−65.15°C, 50 MPa)[37]. A detailed comparison of LDUW and HDUW might provide further insights into their relationships with LDL and HDL.

In summary, we have discovered, by *in situ* optical microscopic observations, that a macroscopic layer and droplets of an unknown form of water with a lower density than that of bulk water can appear at a nonequilibrium water–ice I_h interface. We also succeeded in determining the characteristic velocities of LDUW and HDUW to be about 20 m/s and 100 m/s, respectively. These results suggest that LDUW and HDUW have different local structures from previously observed forms of water, including the quasi-liquid layer at the air–ice I_h interface. Taken in conjunction with our previous observations, which showed macroscopic separation of HDUW from bulk water at the interfaces between water and high-pressure ices III and VI, we have therefore shown that LDUW and HDUW can be observed at nonequilibrium interfaces between water and various forms of ice, in an analogous manner to LDL and HDL, under the conditions far from 'no-man's land'. The macroscopic appearance of LDUW and HDUW with a lifetime observable by conventional optical microscopy is possibly significant for the development of research, not only on the origin of the unique properties of water hidden in the "no-man's land" region, but also the liquid polymorphisms of single-component systems in regions where there are experimental constraints, such as supercooling limits of the pure liquid.

A dynamic sapphire anvil cell electrically-regulated by piezo actuators (d-SAC) was used for the high-pressure experiment (See SI Text S1 for details)[22]. Ultrapure water from an ultrapure-water-producing apparatus (Simplicity UV; Merck Millipore, Burlington, MA, USA) fed with

distilled water (Kyoei Seiyaku Co., Tokyo, Japan) was used as the mother liquid for crystallization of ice I_h. A single crystal of ice I_h in water was repeatedly melted and grown by compression and decompression using the d-SAC in the low-temperature room kept at -10°C. The interface between the water and the ice I_h crystal repeatedly grown and melted in synchronization with (de)compression was observed *in situ* by bright-field microscopy, differential-interference phase-contrast microscopy, and Fizeau-type laser interferometric microscopy using an inverted optical microscope (IX71; Olympus Corp., Tokyo, Japan) located in the low-temperature room.

ACKNOWLEDGMENT

We thank Y. Sato, S. Mori and S. Saito for helping the fabrication of d-SAC. This research was supported by the Grant for Joint Research Program of the Institute of Low Temperature Science, Hokkaido University (18K001) and the Sasakawa Scientific Research Grant from the Japan Science Society (2021-2001).

SUPPORTING INFORMATION (SI)

The Supporting Information is available free of charge on the ACS Publications website at XXXX.

SI Text S1. The details of experimental methods., SI Text S2. Thermodynamic driving force for crystallization by d-SAC., SI Text S3. Estimation of the wetting angle of LDUW at the water–growing ice interface., SI Text S4. Estimation of the maximum possible value for the viscosity of LDUW., SI Text S5. Estimation of the viscosity of bulk water at –10 °C and 107 MPa. SI Text S6. Determination of the characteristic velocity of HDUW at the water–ice III interface., SI Figure S1. Electrically regulated anvil cell with piezo actuator, dynamic sapphire anvil cell (d-SAC). SI Figure S2. Experimental setup of the microinterferometer and in situ observation of the thin layer of LDUW at the water–

growing ice interface with the microinterferometer., SI Figure S3. Estimation of the effective overdepressure at the water–ice I_h interface and the thermodynamic driving force for crystallization produced by the actuating d-SAC., Figure S4. Schematic showing the relationship of the wetting angle of LDUW at the water–ice I_h interface, based on the interval of the interference fringes in the in situ microinterferograms., Figure S5. Pressure dependence of the refractive index of bulk water at 643.847 nm and the temperature dependence of the increment of the refractive index per 0.1 MPa of pressure increment., Figure S6. Dependence of the viscosity of bulk water on the pressure and temperature., Figure S7. Comparison of oxygen–oxygen two-body distribution functions (TBDFs) for LDL, HDL, Ice Ih, Ice III, Ice VI, and supercooled waters under a high pressure., Figure S8. Analysis of nucleation-and-growth-type dewetting dynamics of HDUW at the water–ice III interface., Figure S9. *In situ* microinterferogram of the hole in the HDUW thin layer at the water–ice III interface., Legends for SI Movies S1-S5, SI References (PDF)., SI Movie S1. Appearance of Low-Density Unknown Water at the Interface between Water and Ice I_h Grown by Decompression (MPEG), SI Movie S2. *In situ* Laser-Interferometric Observation of Low-Density Unknown Water at the Interface between Water and Ice I_h Grown/Melted by De/Compression. (MPEG), SI Movie S3. Appearance of Low-Density Unknown Water at the Interface between Water and Ice I_h Melted by Compression. (MPEG), SI Movie S4. Coalescence Dynamics of a Low-Density Unknown Water Droplet with Its Thin Layer. (MPEG), SI Movie S5. Nucleation-and-Growth-Type Dewetting Dynamics of High-Density Unknown Water at Water–Ice III Interface. (MPEG).

Notes

The authors declare no competing financial interest.

REFERENCES

1. Henry, L.; Mezouar, M.; Garbarino, G.; Sifré, D.; Weck, G.; Datchi, F Liquid–liquid transition and critical point in sulfur. *Nature* **2020**, 584, 382–386.
2. Katayama, Y.; Mizutani, T.; Utsumi, W.; Shimomura, O,; Yamakata, M.; Funakoshi, K. A first-order liquid–liquid phase transition in phosphorus. *Nature* **2000**, 403, 170–173.
3. Tanaka, H. Liquid–liquid transition and polyamorphism. 2020, *J. Chem. Phys.* 153, 130901.
4. Tanaka, H.; Tong, H.; Shi, R.; Russo, J. Revealing key structural features hidden in liquids and glasses. *Nat. Rev. Phys.* **2019**, 1, 333–348.
5. Sastry, S.; Angell, C. A. Liquid–liquid phase transition in supercooled silicon. *Nat. Mater.* **2003**, 2, 739–743.
6. Glosli, J. N.; Ree, F. H. Liquid–liquid phase transformation in carbon. *Phys. Rev. Lett.* **1999**, 82, 4659–4662.
7. Morales, M. A.; Pierleoni, C.; Schwegler, E.; Ceperley, D. M. Evidence for a first-order liquid–liquid transition in high-pressure hydrogen from ab initio simulations. **2010**, *Proc. Natl Acad. Sci. USA* 107, 12799–12803.
8. Boates, B.; Bonev, S. First-order liquid–liquid phase transition in compressed nitrogen. *Phys. Rev. Lett.* **2009**, 102, 015701.
9. Murata, K.; Tanaka, H. Microscopic identification of the order parameter governing liquid–liquid transition in a molecular liquid. *Proc. Natl Acad. Sci. USA* **2015**, 112, 5956–5961.
10. Poole, P. H.; Sciortino, F.; Essmann, U.; Stanley, H. E. Phase behaviour of metastable water. *Nature* **1992**, 360, 324–328.

11. Speedy, R. J.; Angell, C. A. Isothermal compressibility of supercooled water and evidence for a thermodynamic singularity at –45 °C. *J. Chem. Phys.* **1976**, 65, 85.

12. Taschin, A.; Bartolini, P.; Fanetti, S.; Lapini, A.; Citroni, M.; Righini, R.; Bini, R.; Torre, R. Pressure effects on water dynamics by time-resolved optical Kerr effect. *J. Phys. Chem. Lett.* **2020**, 11, 3063–3068.

13. Gallo, P.; Winkel, K. A.; Angell, C. A.; Anisimov, M. A.; Caupin, F.; Chakravarty, C.; Lascaris, E.; Loerting, T.; Panagiotopoulos, A. Z.; Russo, J.; Sellberg, J. A. *et al.* Water: A tale of two liquids. *Chem. Rev.* **2016**, 116, 7463–7500.

14. Taschin, A.; Bartolini, P.; Eramo, R.; Righini, R.; Torre, R. Evidence of two distinct local structures of water from ambient to supercooled conditions. *Nat. Commun.* **2013**, 4, 2401.

15. Kringle, L.; Thornley, W. A.; Kay, B. D.; Kimmel, G. A. Reversible structural transformations in supercooled liquid water from 135 to 245 K. *Science* **2020**, 369, 1490–1492.

16. Kim, K. H.; Winkel, K. A.; Giovambattista, N.; Späh, A.; Perakis, F.; Pathak, H.; Parada, M. L.; Yang, C.; Mariedahl, D.; Eklund, T. *et al.* Maxima in the thermodynamic response and correlation functions of deeply supercooled water. *Science* **2017**, 358, 1589–1593.

17. Kim, K. H.; Winkel, K. A.; Giovambattista, N.; Späh, A.; Perakis, F.; Pathak, H.; Parada, M. L.; Yang, C.; Mariedahl, D.; Eklund, T. *et al*. Experimental observation of the liquid–liquid transition in bulk supercooled water under pressure. *Science* **2020**, 370, 978–982.

18. Liu, L.; Chen, S. H.; Faraone, A.; Yen, C. W.; Mou, C. Y. Pressure dependence of fragile-to-strong transition and a possible second critical point in supercooled confined water. *Phys. Rev. Lett.* **2005**, 95, 117802.

19. Soper, A. K. Structures of high-density and low-density water. *Phys. Rev. Lett.* **2000**, 84, 2881.

20. Nilsson, A.; Pettersson, L. G. M.; The structural origin of anomalous properties of liquid water. *Nat. Commun.* **2015**, 6, 8998.

21. Niinomi, H; Yamazaki, T.; Nada, H.; Hama, T.; Kouchi, A.; Okada, J. T.; Nozawa, J.; Uda, S.; Kimura, Y. High-density liquid water at a water–ice interface. *J. Phys. Chem. Lett.* **2020**, 11, 6779–6784.

22. Evans, W. J.; Yoo, C. S.; Lee, G. W.; Cynn, H.; Lipp, M. J.; Visbeck, K. Dynamic diamond anvil cell (dDAC): A novel device for studying the dynamic-pressure properties of materials. *Rev. Sci. Instrum.* **2007**, 78, 073904.

23. Nagata, Y.; Hama, T.; Backus, E. H. G.; Mezger, M.; Bonn, D.; Bonn, M.; Sazaki, G. The Surface of ice under Equilibrium and Nonequilibrium Conditions. *Acc. Chem. Res.* **2019**, 52, 1006–1015.

24. Sazaki, G.; Zepeda, S.; Nakatsubo, S.; Yokomine, M.; Furukawa, Y. Quasi-liquid layers on ice crystal surfaces are made up of two different phases. *Proc. Natl Acad. Sci. USA* **2012**, 109, 1052–1055 (2012).

25. Kim, Y. J.; Lee, Y. H.; Lee, S.; Nada, H.; Lee, G. W. Shock growth of ice crystal near equilibrium melting pressure under dynamic compression. *Proc. Natl Acad. Sci. USA* **2019**, 116, 8679–8684.

26. Young, T. An essay on the cohesion of fluids. *Phil. Trans. R. Soc. London* **1805**, 95, 65–87.

27. Blossey, R. *Thin Liquid Films: Dewetting and Polymer Flow*, Springer: Switzerland, 2012.

28. Murata, K.; Asakawa, H.; Nagashima, K.; Furukawa, Y.; Sazaki, G. In situ determination of surface tension-to-shear viscosity ratio for quasiliquid layers on ice crystal surfaces. *Phys. Rev. Lett.* **2015**, 115, 256103.

29. de Gennes, P. G.; Wyart, F. B.; Qéré, D. *Capillarity and Wetting Phenomena: Drops, Bubbles, Pearls, Waves*, Springer: Switzerland, 2003.

30. Tachibana, S.; Kouchi, A.; Hama, T.; Oba, Y.; Piani, L.; Sugawara, I.; Endo, Y.; Hidaka, H.; Kimura, Y.; Murata, K. *et al.* Liquid-like behavior of UV-irradiated interstellar ice analog at low temperatures. *Sci. Adv.* **2017**, 3, eaao2538.

31. Singh, L. P.; Issenmann, B.; Caupin, F. Pressure dependence of viscosity in supercooled water and a unified approach for thermodynamic and dynamic anomalies of water. *Proc. Natl Acad. Sci. USA* **2017**, 114, 4312–4317.

32. Dehaoui, A.; Issenmann, B.; Caupin, F. Viscosity of deeply supercooled water and its coupling to molecular diffusion. *Proc. Natl Acad. Sci. USA* **2015**, 112, 12020–12025.

33. Vega, C.; McBride, C.; Sanza, E.; Abascal, J. L. F. Radial distribution functions and densities for the SPC/E, TIP4P and TIP5P models for liquid water and ices Ih, Ic, II, III, IV, V, VI, VII, VIII, IX, XI and XII. *Phys. Chem. Chem. Phys.* **2015**, 7, 1450–1456.

34. Soper, A. K. The radial distribution functions of water and ice from 220 to 673 K and at pressures up to 400 MPa. *Chem. Phys.* **2000**, 258, 121–137.

35. Abascal, J. L. F.; Sanz, E.; Fernández, R. G.; Vega, C. A. potential model for the study of ices and amorphous water: TIP4P/Ice. *J. Chem. Phys.* **2005**, 122, 234511.

36. Debenedetti, P. G.; Sciortino, F.; Zerze, G. H. Second critical point in two realistic models of water. *Science* **2020**, 369, 289–292.

399 37. Ma, Z.; Li, J.; Wang, F. Continuous and discontinuous dynamic crossover in supercooled
400 water in computer simulations. *J. Phys. Chem. Lett.* **2015**, 6, 3170–3174.
401

402